www.small-structures.com

Competition for Ion Intercalation in Prussian Blue Analogues as Cathode Materials for Calcium Ion Batteries

Henry R Tinker, Mingrui Li, Ajay Piriya Vijaya Kumar Saroja, Yuhan Liu, Yudong Luo, Wanjun Ren, Runzhe Wei, Yi Lu, Pan He, Yupei Han, Christopher A. Howard, Furio Corà,* and Yang Xu*

With multivalent ion batteries being considered viable post-lithium energy storage technologies, the last few years have seen increasing interest in intercalation type cathode materials for Ca-ion batteries (CIBs). Prussian blue analogues (PBAs) display many positive attributes such as open structural framework, large interstitial sites, and versatile transition metal redox activity. The PBA cathodes reported for CIBs often contain K-ion or Na-ion due to the syntheses involving the use of potassium or sodium hexacyanoferrate. It has been long overlooked whether the presence of K-ion or Na-ion in pristine PBAs could affect the Ca-ion storage in the PBAs when assessing their CIB performance. Through a combined experimental and computational investigation, this work reports that when K⁺/Na⁺ is present in the pristine PBAs, K/Na intercalation is preferred by the PBA structure over Ca intercalation even in the Ca cells. Ca-ion intercalation can be increased when the K⁺/Na⁺ content in the pristine PBAs is reduced, shifting from a K or Na-dominated intercalation process to a Ca/K or Ca/Na co-intercalation process. This work consolidates that PBAs are an interesting and versatile intercalation host for several ions, but investigating PBAs as intercalation cathodes requires careful consideration of all ions present in the battery system.

H. R. Tinker, M. Li, A. P. Vijaya Kumar Saroja, Y. Luo, W. Ren, R. Wei, Y. Lu, P. He, Y. Han, F. Corà, Y. Xu
Department of Chemistry
University College London
London WC1H 0AJ, UK
E-mail: f.cora@ucl.ac.uk; y.xu.1@ucl.ac.uk

Y. Liu
The Electrochemical Innovation Lab
Department of Chemical Engineering
University College London
London WC1E 6BT, UK

C. A. Howard Department of Physics & Astronomy University College London London WC1E 6BT, UK

The ORCID identification number(s) for the author(s) of this article can be found under https://doi.org/10.1002/sstr.202400317.

© 2024 The Author(s). Small Structures published by Wiley-VCH GmbH. This is an open access article under the terms of the Creative Commons Attribution License, which permits use, distribution and reproduction in any medium, provided the original work is properly cited.

DOI: 10.1002/sstr.202400317

1. Introduction

The urgency of developing post-Li battery systems has sparked increasing research on previously underexplored alternative battery chemistries such as those involving other alkali metals (Na and K)[1-3] and multivalent ions (Mg, Ca, and Al).[4-11] Compared to Li, all the considered elements are more abundant by several magnitudes.[12] Because multivalent ions need a lower number of intercalants to achieve the same number of electrons transferred by intercalating Li⁺, using multivalent ions makes it potentially feasible to increase electrochemical capacity of intercalation electrodes and thus to significantly increase the energy density of cells utilizing these electrodes compared to Li cells. Compared to Mg²⁺ and Al³⁺, Ca²⁺ has the additional advantages of (i) higher energy density due to a more negative redox potential (Ca²⁺/Ca vs Mg²⁺/Mg vs Al^{3+}/Al : -2.9 vs -2.4 vs -1.7 V, vs standard hydrogen electrode (SHE)) that should

result in a higher cell voltage, and (ii) faster reaction kinetics because Ca^{2+} should be more mobile in electrode materials due to a lower charge density (charge over size, Ca^{2+} vs Mg^{2+} vs Al^{3+} : 2.0 vs 2.8 vs 5.7 e Å⁻³). The absence of Ca dendrite growth on a metallic Ca anode at realistic current densities makes Ca^{2+} even more attractive, [14] as the risk of short-circuit and thermal runaway is removed.

Identifying suitable intercalation cathode materials to host Ca^{2+} is crucial for Ca-ion batteries (CIBs). Although CIB research is at an early stage, researchers have made progress on materials discovery, reporting a range of cathodes including layered metal oxides, $^{[15,16]}$ Prussian blue analogues (PBAs), $^{[17,18]}$ and chalcogenides, $^{[19,20]}$ as well as a few organic materials. $^{[21,22]}$ Undoubtedly, these cathodes have their respective advantages and disadvantages, but from the standpoint of fundamental scientific research, they diversify the knowledge of materials electrochemistry and foster a balanced pathway to push forward the development of CIBs. $^{[23]}$ PBAs are a particularly interesting family of CIB cathodes. They have a general formula $A_xM[Fe(CN)_6]_{1-\gamma}\cdot\Box_{\gamma}\cdot nH_2O$ (0 < x < 2; $\gamma < 1$), where A represents the intercalating ion, M represents N-coordinated transition metal ion, and \Box represents $[Fe(CN)_6]$ vacancies. The crystal



www advancedsciencenews com



www.small-structures.com

structure of PBAs is characteristic for a three-dimensional (3D) open framework with large interstices to allow the accommodation of ions and their diffusion in three dimensions, as well as small lattice strain during repeated ion intercalation. In combination with the high redox potential of Fe^{2+/3+} and the diversity of transition metal ion M, the structural feature enables quick solid-state diffusion of intercalating ions, making PBAs a favorable cathode choice for a wide variety of post Li-ion batteries.^[24-27] CIB is no exception in this regard, and some of the best cathode performances of CIBs were obtained using PBAs. [21,28,29]

Despite the performance development, the Ca intercalation mechanism in PBAs seems ambiguous from literature, being vastly different from study to study. Synthesis of PBAs almost certainly involves using potassium or sodium hexacyanoferrate (Fe²⁺ or Fe³⁺) as one of the precursors, which inevitably introduces K⁺ or Na⁺ in the as-synthesized PBAs. However, it has long been overlooked how the K⁺ or Na⁺ present in the pristine PBA cathode affects Ca intercalation in a Ca cell. Regarding Kcontaining PBAs, Shiga et al. reported the first demonstration in Ca cells using nonaqueous electrolytes.^[17] K_{0.1}Mn₁Fe_{1.1}(CN)₆ showed two redox pairs, which the authors ascribed to different steps of Ca intercalation into different crystallographic sites in the cathode by referencing an earlier work of aqueous Ca²⁺ electrolytes.^[30] Tojo et al. tested Ca intercalation in K_rNiFe(CN)₆·nH₂O in Ca cells, [31] detecting that Ca content increased after initial discharge (intercalation) and Ca and K contents both decreased after the following charge (deintercalation). The results had no indication of the influence of K⁺ on Ca intercalation because the intercalation process from the 2nd cycle was not investigated. Two reports of KFeFe(CN)6 claimed that after the initial deintercalation, Ca²⁺ replaced K⁺ as the intercalating ion. [21,28] Two recent reports of K_xCuFe(CN)₆ did not acknowledge the potential influence of pre-intercalated K^{+.[18,32]} Compared to K-containing PBAs, there has been very limited work on Na-containing PBAs for CIBs. Ingram et al. demonstrated Ca²⁺ can intercalate in and deintercalate from $Na_xMnFe(CN)_6$ and $Na_xNiFe(CN)_6$, [33,34] and the authors made an effort in showing that residual Na⁺ absorbed on the graphite foil current collector before cycling in the Ca cell can intercalate into the cathode together with Ca²⁺. Although there was no discussion on the influence of Na+ on Ca intercalation, these works hint at an active participation of Na⁺ and K⁺ in the CIB operation.

In this work, we investigate the Ca intercalation mechanism in K- and Na-containing PBA materials through experimental characterization and computational modeling. We reveal the profound effect of the K⁺ and Na⁺ presence in PBAs on the Ca intercalation mechanism. We show that both intercalation of K and Na is preferred over Ca even in a Ca- electrolyte environment. As a result, when testing in Ca cells, intercalation in K- and Na-containing PBAs was dominated by K and Na intercalation, respectively; reducing the initial K and Na content in the PBAs can enhance Ca intercalation. Our investigation provides clarification to the Ca intercalation process in the PBA cathodes, and our results emphasize the importance of taking into consideration preexisting ions in CIB cathode materials when studying intercalation mechanisms. We also highlight the concept of

hybrid cells and co-intercalation in battery research, which can contribute to materials design for divalent ion batteries.

2. Results and Discussion

2.1. Structural Characterization

The PB samples synthesized by using K and Na precursors and denoted as KPB and NaPB, respectively, were characterized by microwave plasma atomic emission spectroscopy (MP-AES, Table S1, Supporting Information), elemental analysis (EA, Table S2, Supporting Information), and TGA (Figure S1, Supporting Information). The composition of KPB and NaPB are estimated to be $K_2Fe[Fe(CN)_6]\cdot 0.44H_2O$ and Na_{1.68}Fe[Fe(CN)₆]_{0.92}·1.63H₂O, respectively. It suggests the use of K citrate is effective in reducing [Fe(CN)₆]⁴⁻ anion vacancies and increasing K content. We examined the crystal structures of the samples by analyzing the XRD patterns. The KPB pattern (Figure 1a) can be indexed to a monoclinic phase (space group $P2_1/n$) and the NaPB pattern (Figure 1b) can be indexed to a mixture of monoclinic (space group $P2_1/n$) and cubic (Fm-3m) phases with a ratio of 85%:15%. Based on the compositions, both XRD patterns were successfully fitted with satisfying R values (Table S3–S5, Supporting Information), confirming that the estimated compositions and refined structures were consistent. The refined structures agree with literature. [35-37] The FT-IR spectra of KPB and NaPB are shown in the top part of Figure 1c,d, respectively. The characteristic Fe hexacyanoferrate bands are seen in both samples, locating at ≈2070, ≈595, and \approx 450 cm⁻¹, corresponding to $v(C \equiv N)$ (KPB: 2069 cm⁻¹; NaPB: 2065 cm⁻¹), v(Fe-C) (KPB: 592 cm⁻¹; NaPB: 592 cm⁻¹) and δ (Fe-C-N) (KPB: 455 cm⁻¹; NaPB: 456 cm⁻¹), respectivelv. [38,39] The red shift of $v(C \equiv N)$ indicates the higher water content in NaPB compared to KPB. This is consistent with previous literature. [40] Also, the noticeable bending mode of water at 1615 cm⁻¹ suggests the higher water content in NaPB than KPB. The Raman spectra of KPB and NaPB are shown in the bottom part of Figure 1c,d, respectively. The peaks in the 450–620 cm⁻¹ range (KPB: 515/589 cm⁻¹; NaPB: 516/591 cm⁻¹) are characteristic for all the Fe-C stretching vibrations of the lattice.[41,42] The peaks in the 190–340 cm⁻¹ range represent the Fe—CN—Fe bond deformation vibrations.^[42] The major peaks in the 2000–2200 cm^{-1} are characteristic CN bond, exhibiting a CN E_{g} vibrational mode at the lower wavenumber (KPB: 2082 cm⁻¹; NaPB: 2110 cm $^{-1}$) and a CN A_{1g} vibrational mode at the higher wavenumber (KPB: 2122 cm $^{-1}$ NaPB: 2134 cm $^{-1}$). [43] Cyanide ligands are coordinated to Fe ions with different oxidation state (Fe^{III/II}-CN-Fe^{III/II}) that influences the wavenumber of vibrational modes. Wavenumber increases upon the increase in the Fe oxidation state, as the higher is the Fe oxidation state, the more effective is the Fe cation to $CN^ \sigma$ -bonding. The lower wavenumbers of KPB compared to NaPB shows the lower average oxidation state of Fe in KPB.[44]

SEM and TEM (including HRTEM) images reveal different morphologies of KPB and NaPB (Figure 2). KPB consists of small nanoparticles with the size in the range of 50–70 nm (Figure 2a). TEM image (Figure 2b) shows the irregular shape of the nanoparticles and their agglomeration. HRTEM image (Figure 2c)

26884062, 2024, 12, Downloaded

from https://onlinelibrary.wiley.com/doi/10.1002/sstr.202400317 by University College London UCL Library Services, Wiley Online Library on [03/11/2025]. See the Terms

on Wiley Online Library for rules of use; OA articles are governed by the applicable Creative Commons

www.small-structures.com

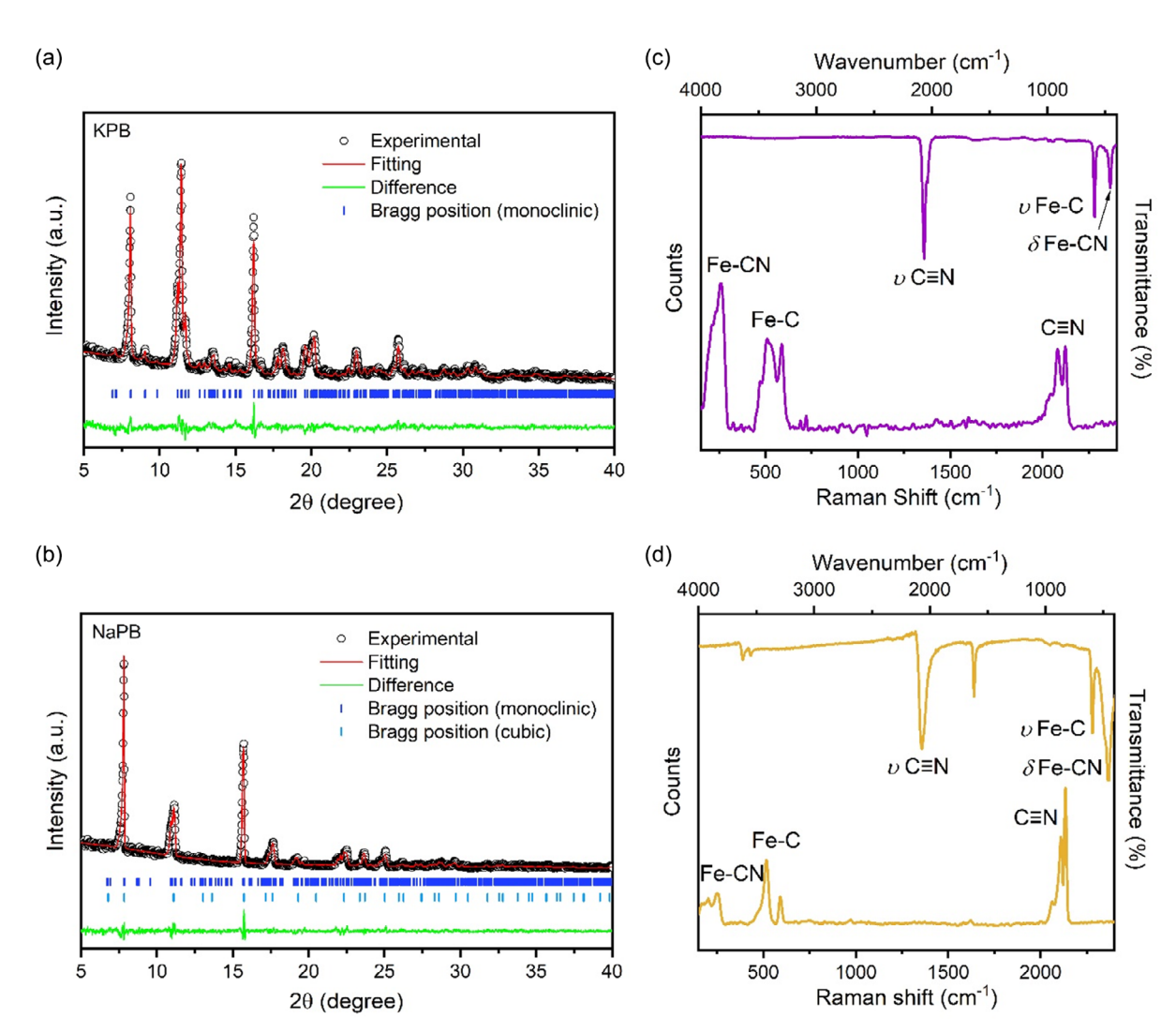


Figure 1. Experimental and refined XRD patterns of a) KPB and b) NaPB. FT-IR and Raman spectra of c) KPB and d) NaPB (top: FTIR; bottom: Raman).

displays lattice fringes with the d spacings of 4.51, 4.52, and 5.10 Å, corresponding to the (111), (-111), and (011) planes, respectively. The different d spacings are due to the nonuniform oriented growth of the nanoparticles; nevertheless, the crystalline nature of the nanoparticles is evidenced. NaPB displays a cubic morphology, and the sizes of the cubes are in the range of 1–3 μ m (Figure 2d,e). Due to the size and thickness, diffractions were taken from small segments (inset in Figure 2e) peeled off from the cubes. The concentric diffraction rings can be assigned to the (200) and (420) planes (Figure 2f).

2.2. Ion Intercalation Mechanisms

We first tested as-synthesized KPB directly as a Ca cathode in Ca cells using $1 \,\mathrm{M}$ Ca(ClO₄)₂ in ACN as the electrolyte, ACC as the counter/reference electrode, and in the voltage range of $-0.6-1.1 \,\mathrm{V}$ (vs. ACC). The potential of ACC was calibrated to be 0.28 V versus SHE by using ferrocene redox pair (Figure S2, Supporting Information). **Figure 3**a shows the CV curves of KPB in the initial three cycles. KPB shows two reduction

(intercalation) peaks at 0.51 and -0.12 V, and the corresponding oxidation (deintercalation) peaks are at 0.63 and 0 V, respectively. The two pairs of peaks are well defined and overlap well in the following cycles, suggesting a two-step ion intercalation process in KPB consisting of the reduction of low-spin (LS) Fe at the higher voltage and the reduction of the high-spin (HS) Fe at the lower voltage. [45] Although the two redox pairs agree with previous literature of K-containing PBAs in Ca cells, [17,21,28] unlike the literature, at this stage we are cautious to assign the redox peaks to Ca intercalation, as we will discuss later, there might be other ion(s) competing with Ca²⁺ or even dominating the intercalation. Interestingly, the intercalation peak voltages 0.51/-0.12 V versus ACC in this work $(3.72/3.09 \text{ V} \text{ vs K}^+/\text{K})$ closely resemble the ones of K intercalation in KPB (3.80/3.11 V vs K⁺/K) from previous reports.^[36] We tested the KPB sample in K cells (Figure S3, Supporting Information), and indeed K intercalation peaks are at 3.70 and 3.08 V versus K+/K (0.49 and -0.13 V vs ACC), which are close to the ones seen in the Ca cell and shown in Figure 3a. The GCD curves of KPB at 30 mA g^{-1} (Figure 3b) exhibit two discharge (charge) plateaus that align well

26884062, 2024, 12, Downloaded from https://onlinelibrary.wiley.com/doi/10.1002/ssr.202400317 by University College London UCL Library Services, Wiley Online Library on [03/1/2025]. See the Terms and Condit.

s) on Wiley Online Library for rules of use; OA articles are governed by the applicable Creative Commons License

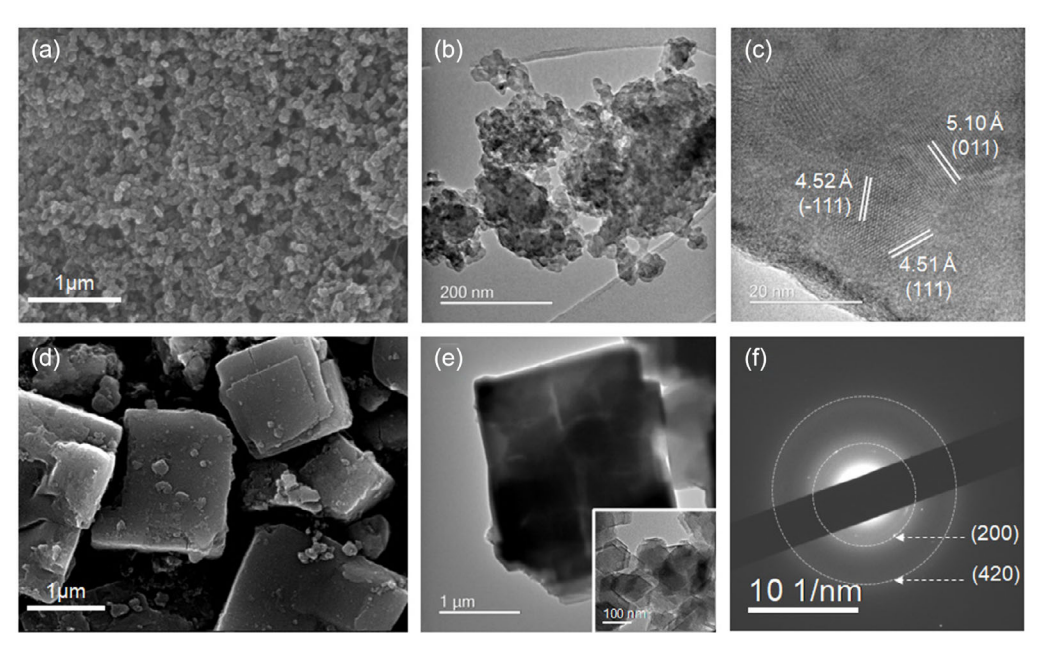


Figure 2. a,d) SEM and b,c,e,f) TEM images of KPB (a-c) and NaPB (d-f). The inset in (e) shows the small segments taken for the diffraction in (f).

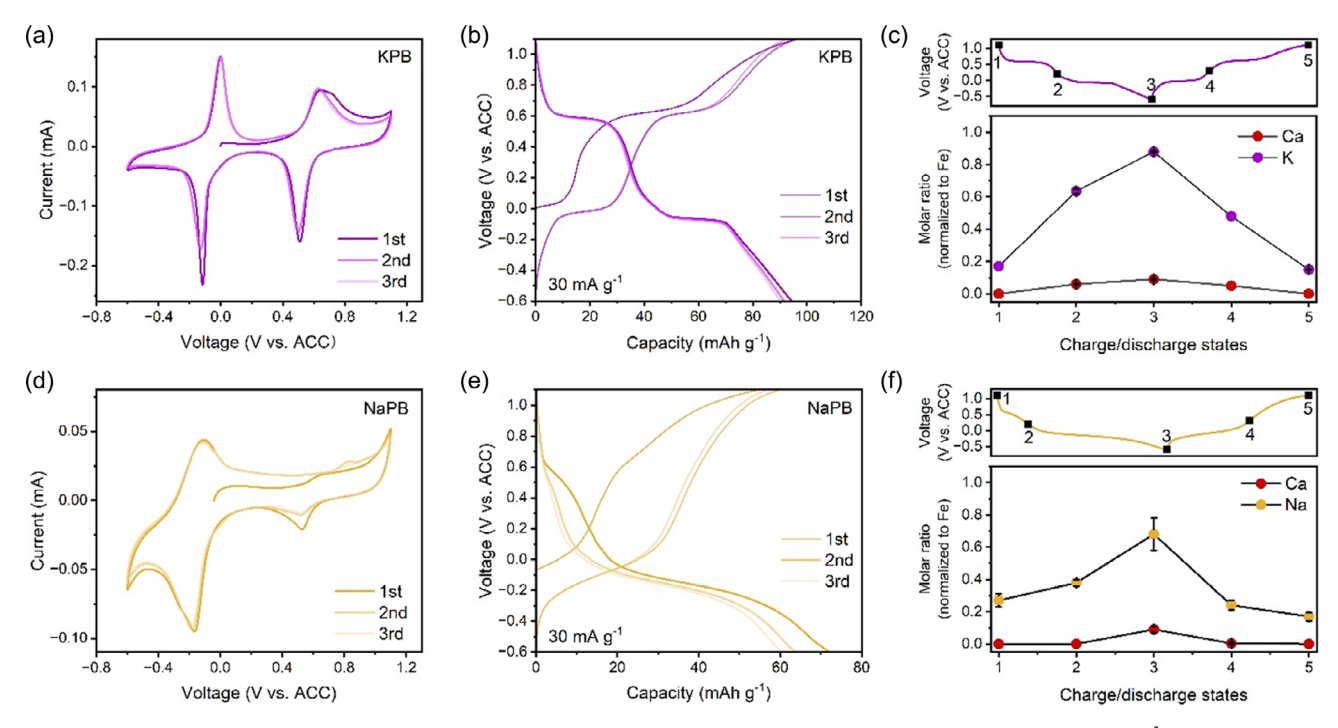


Figure 3. CV curves a,d) and GDC profiles b,e) of KPB (a,b) and NaPB (d,e) in the first three cycles at the current density of 30 mA g^{-1} in the voltage range of -0.6-1.1 V. Ca and K contents in KPB c) and Ca and Na contents in NaPB f) at various charge and discharge states in the first cycle. The contents are normalized to Fe.

with the CV curves. The average discharge and charge capacities of the first three cycles are 92.0 and 94.7 mAh g⁻¹, respectively, at 30 mA g⁻¹. Intrigued by the resemblance of intercalation potentials and voltage profiles of KPB in Ca and K cells (Figure 3a and S3, Supporting Information),^[25,36] we measured the Ca and K contents (normalized to Fe) of the KPB electrodes during

a complete cycle in the Ca cell (the 1st discharge and 2nd charge) by using energy dispersive spectroscopy (EDS), and the results are shown in Figure 3c. The (de)intercalation process is completely dominated by K^+ with a very small contribution from Ca^{2+} . The K/Fe ratio increases almost linearly from 0.17 to 0.88 during discharge (point $1\rightarrow 3$) and decreases to 0.15 during

small structures

www.advancedsciencenews.com www.small-structures.com

charge (point $3 \rightarrow 5$), whereas the Ca/Fe ratio changes slightly, reaching only 0.1 at the end of discharge. The charging cutoff voltage was limited to 1.1 V versus ACC due to the breakdown of ACN at a higher voltage, and thus we were not able to fully depotassiate KPB (K/Fe ratio = 0.17 at point 1) after the initial charge; nevertheless, the vastly different variations in K and Ca contents demonstrate that even though K⁺ (initially preintercalated in KPB during synthesis, i.e., in the pristine KPB) is released into the Ca electrolyte after the initial charge and its concentration is significantly lower than Ca²⁺ in the electrolyte, subsequent intercalation cycles into KPB are dominated by K⁺, suggesting a strong thermodynamic preference for K⁺ compared to Ca²⁺ by the PB framework.

We carried out similar tests on NaPB in Ca cells and compare results to those for KPB. The CV curves (Figure 3d) show a weak reduction peak at $0.52 \,\mathrm{V}$ and a strong reduction peak at $-0.17 \,\mathrm{V}$. The corresponding oxidation peaks are at 0.81 and -0.10 V, respectively. The GCD curves (Figure 3e) agree reasonably well with the CV curves. The first discharge curve shows a slope in the 0.1-0.6 V range and a defined plateau at \approx -0.20 V, with the former becoming weaker in the following cycles. The 1st and 2nd charge/discharge capacities are 54.6/72.1 and $59.9/63.8 \,\mathrm{mAh}\,\mathrm{g}^{-1}$, respectively. Therefore, the performance of NaPB is worse than KPB, presumably due to the much large particle size of the former (a few µm vs 50-70 nm), which worsens ion diffusion kinetics in NaPB. We tested NaPB in Na cells (Figure S4, Supporting Information), and the discharge curves show a semi-plateau in the 3.20-3.70 V range and a more defined plateau around 2.80 V versus Na⁺/Na. The voltages are close to the ones shown in Figure 3e, 0.1-0.6 V range versus ACC $(3.09-3.59 \text{ vs } \text{Na}^+/\text{Na}) \text{ and } -0.20 \text{ V versus ACC } (2.79 \text{ V vs})$ Na⁺/Na). Same as K, Ca, and Na contents (normalized to Fe) were measured during a complete cycle by using EDS to investigate ion intercalation (Figure 3f), and the results show that the intercalation process is dominated by Na+. The Na/Fe ratio increases almost linearly from 0.27 to 0.68 during discharge (point $1\rightarrow 3$) and decreases to 0.17 during charge (point $3\rightarrow 5$), whereas the Ca/Fe ratio remains very low, reaching only 0.1 at the end of discharge. Comparing the behavior of NaPB (Figure 3f) with KPB (Figure 3c), we notice that more Na⁺ remains in NaPB than K⁺ in KPB at the beginning of charge, and less Na intercalates than K⁺ at the end of discharge. This observation could be due to the much larger particle size of NaPB than KPB, leading to more sluggish ion diffusion kinetics. Nevertheless, the same conclusion could be drawn for NaPB and KPB: even though the Ca electrolyte has much higher concentration of Ca²⁺ than Na⁺ or K⁺ (the latter only being released from the as-synthesized NaPB and KPB in the initial charge process), intercalation in NaPB and KPB is dominated by Na⁺ and K⁺, respectively, suggesting a lower propensity of the PB host lattice to intercalate Ca²⁺ compared to both Na⁺ and K⁺.

To validate the above observations, in the next step of our work, we aimed at producing a PBA host for Ca that is free of K and Na by extracting K⁺/Na⁺ from KPB/NaPB in a separate cell and then testing the depotassiated/desodiated PB in a fresh Ca cell. The depotassiated and desodiated samples are denoted as DeK PB and DeNa PB, respectively. As shown in **Figure 4a**,b, the CV and GCD curves of DeK PB show significant differences compared to those of KPB. The LS Fe reduction peak at 0.55 V is weakened, and the HS Fe reduction peak shifts to a

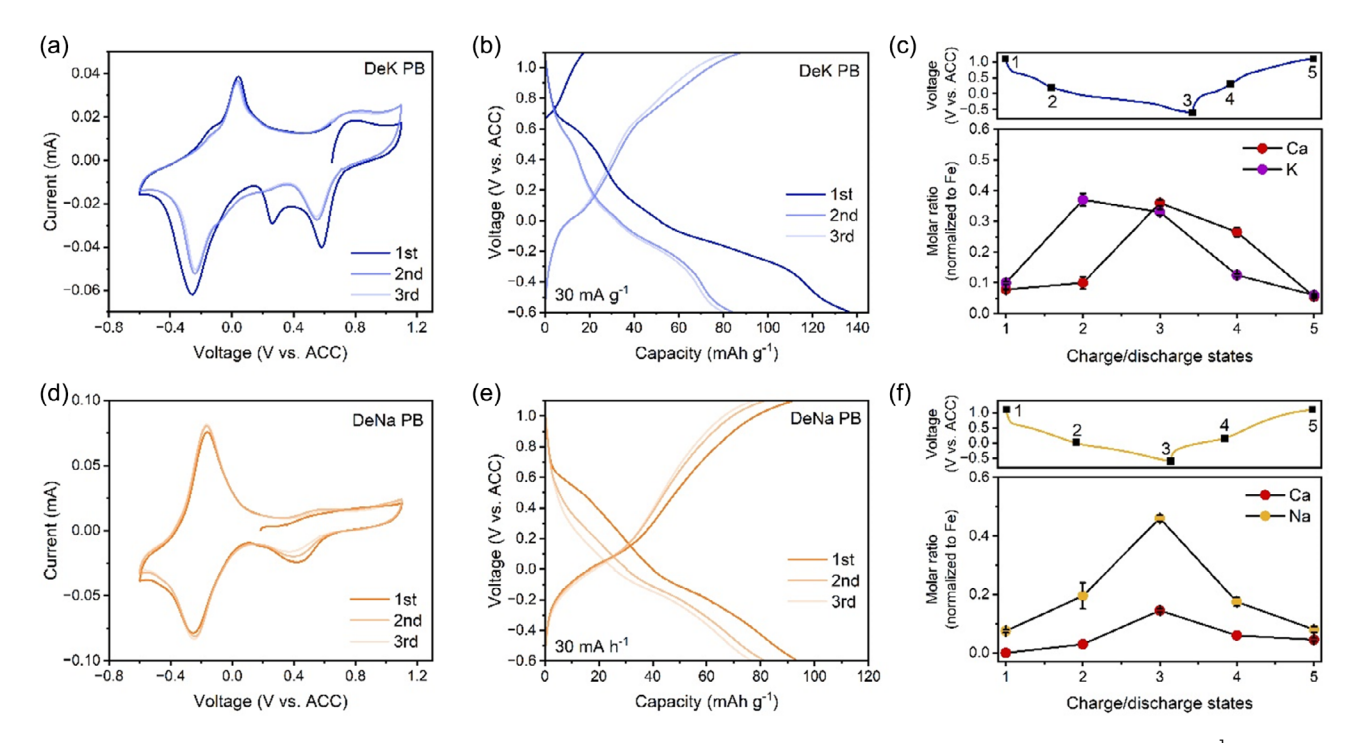


Figure 4. CV curves a,d) and GDC profiles b,e) of DeK PB (a,b) and DeNa PB (d,e) in the first three cycles at the current density of 30 mA g^{-1} in the voltage range of -0.6-1.1 V. Ca and K contents in DeK PB c) and Ca and Na contents in DeNa PB f) at various charge and discharge states in the first cycle. The contents are normalized to Fe.

www.advancedsciencenews.com

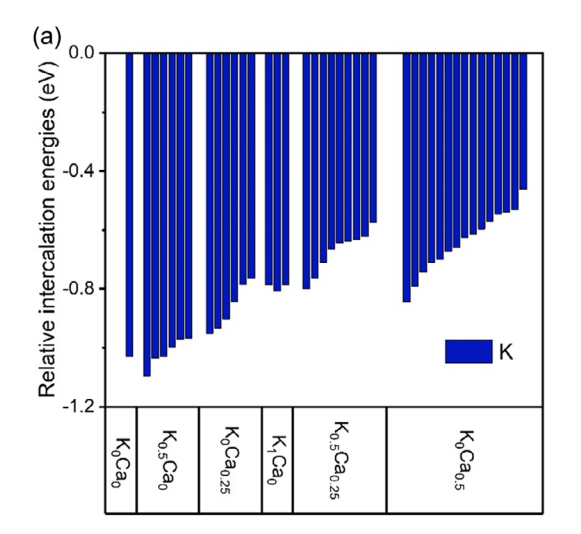
www.small-structures.com

lower voltage of -0.26 V. Both peaks are broader than those for KPB in Figure 3a. As a result, the GCD curves become sloping, and the high-voltage slope is reduced compared to the curves in Figure 3b. The more sloping discharge plateaus could be due to two reasons. First, Ca and K intercalation occupies different sites in the PBA framework from the thermodynamic point of view, leading to different energies required for the intercalation. Second, Ca diffusion may have more sluggish kinetics due to the bivalence and thus potentially a higher overpotential compared to K diffusion. The capacity of the 2nd and 3rd cycle is \approx 82 mAh g⁻¹ for DeK PB, close to that of KPB. The measured Ca/Fe and K/Fe ratios of DeK PB during a complete cycle in the Ca cell are shown in Figure 4c. We observed different results compared to KPB. Some K is still present in the DeK PB sample, and as previously explained, it is because the maximum voltage that can be applied before decomposition of the ACN electrolyte does not enable full removal of K. The K/Fe ratio rises to 0.37 in the 1st intercalation step (point $1\rightarrow 2$), but the Ca/Fe ratio increases only slightly, which indicates the 1st ion intercalated is still K⁺. Upon continuing discharge (i.e., further intercalation into DeK PB, point $2\rightarrow3$), once K⁺ is consumed from the electrolyte, we do observe the Ca content to increase, reaching a Ca/Fe ratio of 0.36 at fully discharge state. This ratio is much higher than the one at the same stage in KPB. Both Ca/Fe and K/Fe ratios gradually decrease during charge (point $3\rightarrow 5$), with first Ca content decreasing slower than K (point $3\rightarrow 4$) and then K content decreasing slower than Ca (point $4\rightarrow 5$). The initial K/Fe ratio of DeK PB prior to the Ca cell test is 0.42, suggesting the depotassiation in the separate cell was incomplete; however, the K content of 0.1 after the initial charge process in the Ca cell is lower than that in KPB. The significant reduction of K content in DeK PB compared to KPB results in a significant reduction of K⁺ entering the Ca electrolyte after the initial charge. The observations suggest that possibly due to the strong preference of K⁺ over Ca²⁺ in the PB framework, reducing the presence of K⁺ in the Ca cell does enhance Ca intercalation. Based on this result, it is worth emphasizing that when applying K-containing PB as a cathode material for CIBs, care needs to be taken to interpret intercalation mechanisms and prove the exclusivity of Ca intercalation.

The CV (Figure 4d) and GCD curves (Figure 4e) describing the application of DeNa PB in the Ca cell are similar to those of NaPB (Figure 3d,e) in terms of peak positions and voltage profile. A weak/strong intercalation peak remains at $\approx 0.5/\approx -0.2 \,\mathrm{V}$. The GCD curves show a sloping feature with an ill-defined separation of the two intercalation steps around $-0.1\,\mathrm{V}$. Figure 4f shows the Ca/Fe and Na/Fe ratio changes during (de)intercalation. Compared to NaPB (Figure 3f), DeNa PB shows the gradual increase/decrease in Ca and Na contents during discharge/ charge. At fully discharged state (point 3), the Ca/Na ratio is higher in DeNa PB (0.15/0.46 = 1/3) than in NaPB (0.10/10.46 = 1/3)0.68 = 1/7). This indicates that even partially removing Na⁺ from the starting PB material (Na/Fe ratio was 0.5 after the desodiation in the separate cell) enhances the amount of Ca intercalation. It is safe to conclude that the presence of Na⁺ affects Ca intercalation in the Ca cells, and similar to using K-containing PB cathodes, using Na-containing PB as a cathode material for CIBs requires careful investigation of intercalation mechanisms.

2.3. Computational Investigation

To quantify the energies and dynamics of Na, K, and Ca intercalation in PB, we carried out a computational investigation using density functional theory (DFT) calculations. We first discuss how the competitive intercalation of Na, K, and Ca dissolved in a common electrolyte was simulated. Calculation of the absolute intercalation voltage of Na, K, or Ca requires a description of the reaction at the anode, which releases electrons toward the cathode and cations into the electrolyte. Since the three cations were dissolved in the same electrolyte and the same reaction took place at the ACC anode irrespective of the ion intercalating in the PB cathode, the energy contribution of the reaction at the anode can be cancelled out by calculating the relative intercalation energy E^{R} of Na, K, Ca in M_{r}^{I} Ca_rFeFe(CN)₆ (M = Na, K). E^R was obtained via subtracting the energy of intercalating M^I (the average energy of intercalation sites) by the energy of intercalating Ca (the energy at the most stable intercalation site) for all PB compositions $M_x^I Ca_y Fe Fe (CN)_6$ examined, where x and y quantify the amount of preexisting M^I and/or Ca in the structure. A negative E^{R} means M^{I} intercalation is preferred over Ca intercalation, while a positive E^{R} means the opposite; thus, E^{R} illustrates the preference of intercalating Na/K versus Ca. Various PB compositions corresponding up to 50% Fe reduction (1 Fe per formula) were considered, including FeFe(CN)₆ $(x = 0, y = 0, 0\%), M_{0.5}^{1} \text{FeFe(CN)}_{6} (x = 0.5, y = 0, 25\%),$ $Ca_{0.25}FeFe(CN)_6$ (x = 0, y = 0.25, 25%), $M_1^IFeFe(CN)_6$ (x = 1, y = 0, 50%), $M_{0.5}^{I}$ Ca_{0.25}FeFe(CN)₆ (x = 0.5, y = 0.25, 50%), and $Ca_{0.5}FeFe(CN)_{6}$ (x = 0, y = 0.5, 50%). Figure 5a,b show E^{R} for K and Na, using the Ca intercalation energy at the most stable site as reference for each M^I_xCa_vFeFe(CN)₆. The calculated values of E^R are provided in Table S6, Supporting Information, and Ca intercalation energies in all sites relative to the energy at the most stable site are provided in Figure S5, Supporting Information. E^{R} for K is negative across all the PB compositions considered, suggesting that independently on initial composition of the PB cathode, K intercalation is favorable over Ca, in agreement with the experimental results discussed for KPB and DeK PB, where K dominates the intercalation process in the Ca cell. The preference for K over Ca decreases with the discharge process proceeding. Upon increasing the content of intercalated ions, the absolute value of E^{R} decreases (from -1 eV at x = 0, y = 0 - -0.6 eV at x = 1, y = 0), implying that Ca intercalation becomes more significant nearing the completion of K intercalation, consistent with the results of DeK PB in Figure 4c. ER for Na is once again negative across all the PB compositions calculated, suggesting Na intercalation is preferred over Ca in support of the analysis for Figure 3f. However, E^{R} for Na is less negative than that for K, indicating a less pronounced thermodynamic preference for Na than for K over Ca. E^{R} becomes much less negative with increasing Fe reduction level. This implies the preference of Na intercalation reduces significantly when more Fe is reduced, which supports the co-intercalation of Na and Ca discussed in the analysis of Figure 4f, in comparison to the more staggered K/Ca intercalation. Overall, our calculations clearly demonstrate that K and Na intercalation are both preferred over Ca. Consequently, care needs to be taken when interpreting Ca intercalation mechanisms in PBAs when www.advancedsciencenews.com www.small-structures.com



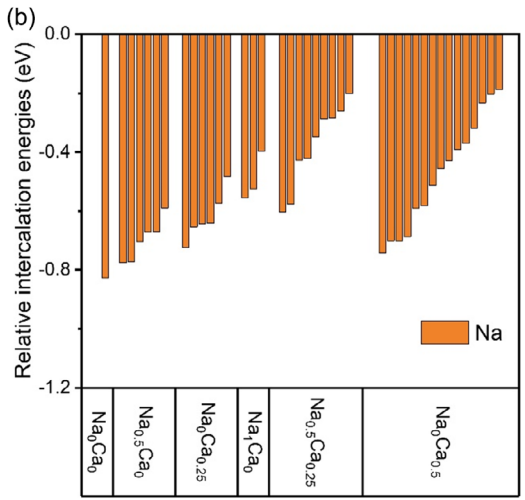


Figure 5. Relative intercalation energy E^R of K intercalation a) and Na intercalation b) to Ca intercalation at various PB compositions M_xCa_yFeFe(CN)₆.

other ions derived from the as-synthesized cathode are present in the Ca cell.

The energy barrier for migration of Na, K, and Ca in PB was calculated to elucidate the effect of diffusion kinetics on the experimental observations. We defined three sites in the Fe₈(CN)₁₂ sub-cubes formed by Fe at the corners and CN ligands along each edge (Figure S6a, Supporting Information): A is a cuboctahedral site in the center of the sub-cubes: B is a window site in the center of the square windows formed by Fe-CN-Fe and connecting adjacent A site along the <100> direction; C is an off-center site connecting site A with the corner of the sub-cube along the <111> direction. The most stable intercalation site for the larger sized K ion was found to be close to the A site, slightly displaced toward site C (Figure S6b, Supporting Information). The presence of K in the PB interstices causes a tilting of the FeN₆ and FeC₆ octahedra. The most stable site for the smaller Na and Ca ions at a low intercalation level (<50% site occupancy) was found to be close to site B, \approx 0.6 Å away from the square window plane containing the Fe ions (Figures S6c,d, Supporting Information). The presence of Na and Ca ions in this site causes in-plane tilting of the Fe(CN)₆ octahedra that shifts the N end of the CN ligands toward the intercalated ion. The stable sites and diffusion following intercalation obviously affect the migration profiles and energy barriers (Figure S7a, Supporting Information). Na ion migrates from a B site in the <100> direction through rolling around one CN ligand to occupy a new B site in the bottom square window (Figure S7b, Supporting Information). This migration yields a new minimum at the normalized coordinate n = 0.5 and a small barrier of 0.13 eV. Ca ion shares a similar migration profile to Na ion (Figure S7c, Supporting Information), but it has a higher barrier of $0.53 \, \text{eV}$ at n = 0.5 because it causes a more pronounced tilting distortion of the square window at x = 0 compared to Na ion, and it cannot occupy the bottom square window at n = 0.5due to its larger size compared to Na ion. K ion is stable at C site and thus migrates through the center of the sub-cube (Figure S7d, Supporting Information), showing a barrier of $0.66 \,\mathrm{eV}$ when crossing the square windows (n = 0 and 1).

The fact that Na and Ca ions have similar intercalation sites and follow a similar migration path may imply a stable co-intercalation of Na and Ca due to similar in-plane tilting. Although the K migration has a higher energy barrier for diffusion in PB, it may be offset by the stronger intercalation energy when competing with Ca (or Na) for intercalation from the electrolyte. How the interplay between K migration energy barrier and intercalation energy determines the overall behavior requires further investigation.

2.4. Further Electrochemical Tests

We cycled DeK PB and DeNa PB at 30 mA g⁻¹ for 30 cycles to further probe the ion intercalation process. Figure 6a shows the GCD curves of cycle30 of the two samples. Both discharge curves kept their features reasonably well compared to their respective curve of cycle1 (Figure 4b,e). For DeK PB, the two slopes at the higher and lower voltage ranges are visible (compared to Figure 4b). For DeNa PB, the curve is declined above $-0.2\,\mathrm{V}$ compared to the initial cycles (Figure 4e), resulting in a reduced capacity. Ca/K/Na content was tested after 30 cycles (Figure 6b) and compared to the initial cycle. For DeK PB, at the discharged state to $-0.6\,\mathrm{V}$ (intercalation), the Ca/Fe ratio increases to 0.40 and the K/Fe ratio decreases to 0.25, showing that despite K⁺ possibly being the favorable intercalant, Ca intercalation exceeds K intercalation over cycles (Figure 4c), shifting the intercalation toward Ca²⁺. The increase in Ca intercalation is more obvious for DeNa PB. Ca content is more than twice as much as Na content at the discharged state after 30 cycles, which is much higher than 0.33 (Ca/Na) at cycle1 (Figure 4f). We acknowledge that ion intercalation in a PB framework can be affected by many factors, particularly considering Ca2+ as a divalent intercalant has a strong charge interaction with the PB structure and sluggish diffusion kinetics, and therefore, the cycles at which Ca intercalation exceeds K/Na intercalation may differ from one PBA host to another; however, the results here once again demonstrate that studying PBAs for CIBs should carefully consider the cations present in the cell beside Ca²⁺, and Ca intercalation in PBAs

26884062, 2024, 12, Downloaded from https://onlinelibrary.wiley.com/doi/10.1002/sstr.202400317 by University College London UCL Library Services, Wiley Online Library on [03/11/2025]. See the Terms and Conditions (https://online.library.wiley.com/doi/10.1002/sstr.202400317 by University College London UCL Library Services, Wiley Online Library on [03/11/2025]. See the Terms and Conditions (https://online.ibrary.wiley.com/doi/10.1002/sstr.202400317 by University College London UCL Library Services, Wiley Online Library on [03/11/2025]. See the Terms and Conditions (https://online.ibrary.wiley.com/doi/10.1002/sstr.202400317 by University College London UCL Library Services, Wiley Online Library on [03/11/2025]. See the Terms and Conditions (https://online.ibrary.wiley.com/doi/10.1002/sstr.202400317 by University College London UCL Library Services, Wiley Online Library on [03/11/2025]. See the Terms and Conditions (https://online.ibrary.wiley.com/doi/10.1002/sstr.202400317 by University College London UCL Library Services, Wiley Online Library on [03/11/2025]. See the Terms and Conditions (https://online.ibrary.wiley.com/doi/10.1002/sstr.202400317 by University College London UCL Library Services, Wiley Online Library on [03/11/2025]. See the Terms and Condition (https://online.ibrary.wiley.com/doi/10.1002/sstr.202400317 by University College London UCL Library Services, Wiley Online Library on [03/11/2025]. See the Terms and Condition (https://online.ibrary.wiley.com/doi/10.1002/sstr.202400317 by University College London (https://online.ibrary.wiley.com/doi/10.1002/sstr.2024

nditions) on Wiley Online Library for rules of use; OA articles are governed by the applicable Creative Commons

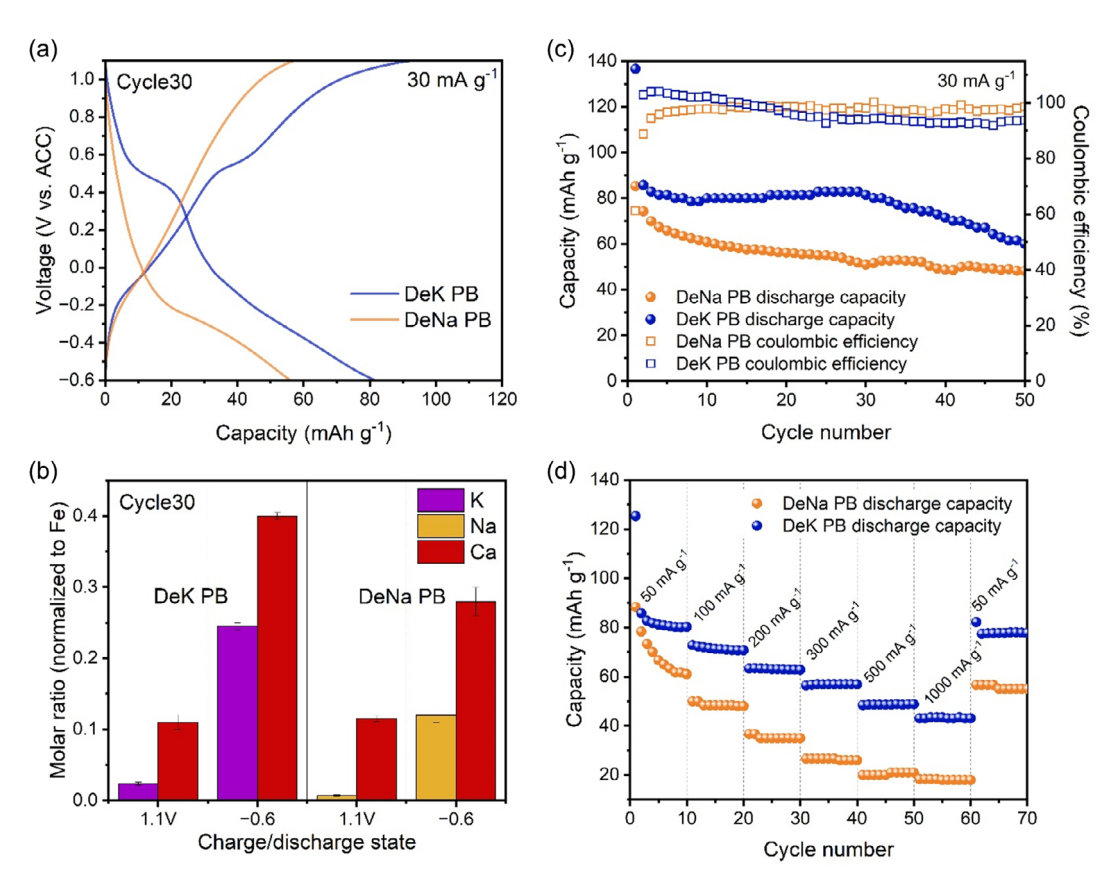


Figure 6. GDC profiles a), Ca and K contents in DeK PB and Ca and Na contents in DeNa PB b) at Cycle30. Cycling performance at 30 mA g^{-1} c) and rate capability d) of DeK PB and DeNa PB.

must be proven. As shown in Figure 6c, DeNa PB delivers a capacity of $56.0 \,\mathrm{mAh}\,\mathrm{g}^{-1}$ after 30 cycles, keeping 69% of the capacity at cycle2, while DeK PB delivers a higher capacity of 81.7 mAh g⁻¹, corresponding to a higher capacity retention of 99% compared to DeNa PB, which is comparable to previous reports on K-containing PBAs. [21,28] The capacity of DeK PB starts decaying after 30 cycles, which suggests cycling stability over a longer term will need to be improved in the future, for instance, by developing better Ca electrolytes. DeK PB also exhibits better rate capability (Figure 6d), retaining capacities of 80, 71, 63, 57, 49, and 43 mAh g^{-1} at 50, 100, 200, 300, 500, and 1000 mA g^{-} respectively, and recovering 78 mAh g⁻¹ when returning to $50\,\mathrm{mA\,g^{-1}}$. In contrast, DeNa PB retains a lower capacity at all tested current densities with the values of 78, 50, 36, 26, 20, 18 mAh g⁻¹ at 50, 100, 200, 300, 500, and 1000 mA g⁻¹, respectively. Rate capability has been rarely demonstrated for PBA cathodes in CIBs with non-aqueous electrolytes, and to the best of our knowledge, the rate capability shown here is among the best so far. $^{[18,28,\widetilde{29},32]}$ It is interesting to see the presence of K^+ , in comparison to Na⁺, might enhance the CIB performance to some extent, particularly the rate capability. We suspect Ca/K co-intercalation might have a positive effect on improving Ca diffusion kinetics. An in-depth investigation is needed to understand the effect; however, it is outside of the scope of this work.

To further examine the intercalation process in DeK PB and DeNa PB, we carried out additional measurements. **Figure 7**a,c

show the CV curves of DeK PB and DeNa PB, respectively, collected at scan rates from 0.1 to 1.0 mV s⁻¹. The linear fitting is shown in Figure 7b (DeK PB) and 7d (DeNa PB). All the reduction (Re) and oxidation (Ox) peaks are identifiable and reversible, with peak shape and voltage separation of Re/Ox peaks almost unchanged upon increasing scan rate. The peak currents shown in Figure 7b.d increase almost linearly to the square root of the scan rate (R^2 value of the linear fitting: DeK PB – Ox 1st: 0.992; Ox 2nd: 0.959; Re 1st: 0.999; Re 2nd: 0.972; DeNa PB - Ox 1st: 0.997; Ox 2nd: 0.995; Ox 3rd: 0.996; Re 1st: 0.998; Re 2nd: 0.993). This suggests diffusion-controlled reduction (intercalation) and oxidation (deintercalation) processes in both samples. We attempted to estimate the diffusion coefficient (D) in DeK PB and DeNa PB based on the slopes obtained from the linear fitting and the Randles-Sevcik equation. [46] Given that K/Ca and Na/Ca co-intercalation take place in DeK PB and DeNa PB, respectively, this analysis cannot give an accurate D value of Ca diffusion but rather aims to compare ion diffusion rates between the two samples. We chose the Re 1st peak for the estimation because the corresponding intercalation step showed higher Ca content increase compared to the Re 2nd peak, particularly for DeK PB. Noted that the equation contains ion concentration (in mol cm⁻³), which was difficult to accurately estimate due to the nonstoichiometry of DeK PB and DeNa PB. Nevertheless, the estimation resulted in the D value at the magnitude of 10^{-10} for both samples, being comparable to previous reports. [29]

on Wiley Online Library for rules of use; OA articles are governed by the applicable Creative Commons

www.small-structures.com



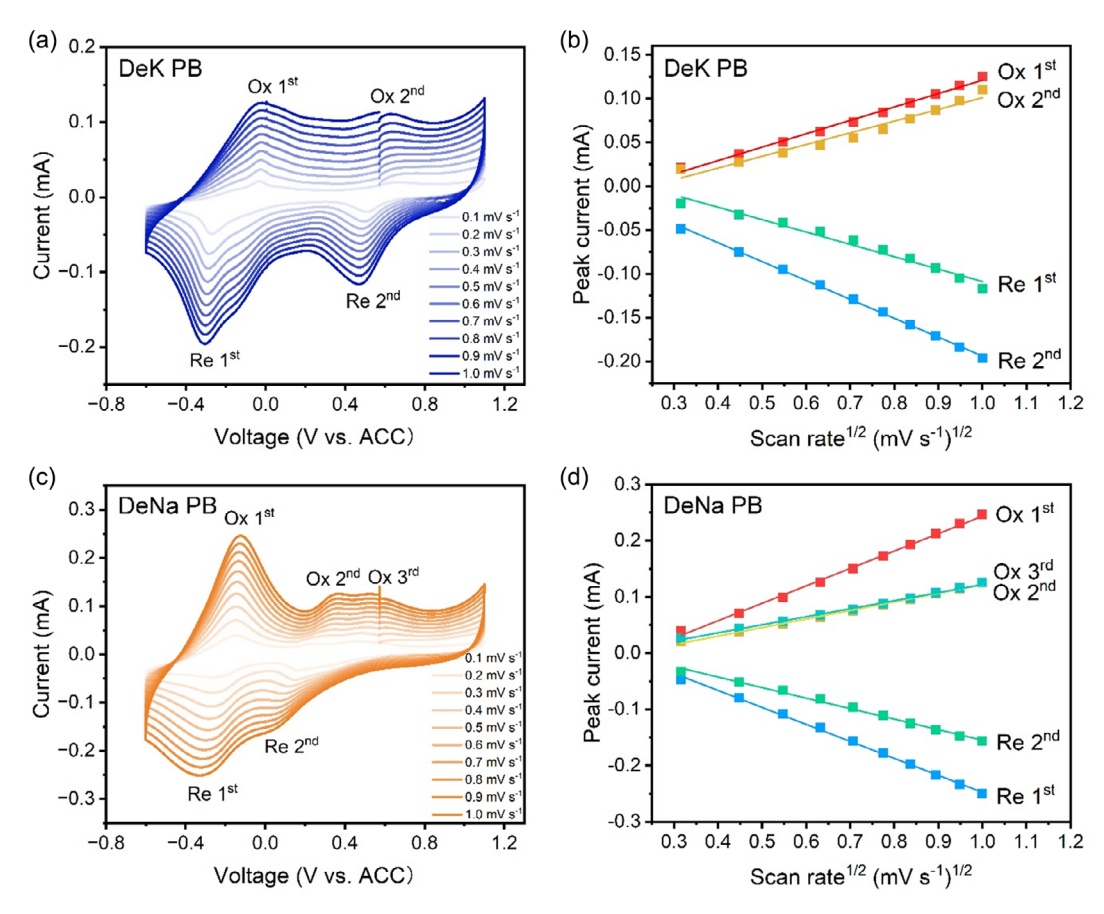


Figure 7. CV curves of a) DeK PB and c) DeNa PB at various scan rates. The linear fitting between peak current and the square root of scan rate for b) DeK PB and d) DeNa PB.

Raman spectra of DeK PB (Figure S8, Supporting Information) and DeNa PB (Figure S9, Supporting Information) at various discharge and charge states were collected as another support to evidence ion intercalation. The reversible peak shift of the CN stretching modes in 2050–2200 cm⁻¹ proves the reversible Fe reduction and oxidation in the two samples, indicating reversion ion (de)intercalation.

3. Conclusions

In summary, we carried out a mechanistic study on the Ca intercalation process in the PB cathodes that contain either K or Na ion from the synthesis of the cathodes. Our work revealed that K and Na are the preferred intercalants compared to Ca, and K or Na intercalation was the dominating processes in the K-containing or Na-containing PBAs, respectively, contributing the majority capacity in the Ca cells. Reducing the initial K/Na content in the PBAs increased the capacity contribution of Ca intercalation. Computational investigation confirmed that not only are K and Na intercalation preferred over Ca intercalation at various PB compositions, but also the preference of K intercalation is stronger than that of Na intercalation. The DeK PB cathode with a reduced K content delivered capacities of 82 mAh g $^{-1}$ at $30~{\rm mA~g}^{-1}$ and $43~{\rm mAh~g}^{-1}$ at $1000~{\rm mA~g}^{-1}$, among the best

rate capability of the PBA cathodes for CIBs so far. Other than the specific K/Ca and Na/Ca systems, our work sheds light on battery systems with mixed ions and shows the importance of clarifying the intercalation mechanisms at the atomic level to design materials with the best-in-class performance.

4. Experimental Section

Materials Synthesis: The PBA samples were synthesized via citrate-assisted coprecipitation. In a typical synthesis of the K-containing PBA sample, 2.5 mmol of $K_4 Fe(CN)_6 \cdot 3H_2O$ with 10 mmol of $C_6H_5K_3O_7$ was dissolved in 50 mL of DI water (Solution A), while 2.5 mmol of FeSO4 \cdot 7H₂O with 10 mmol $K_3C_6H_5O_7$ (potassium citrate) was dissolved in a separate 50 mL of DI water (Solution B). Solution B was slowly added to Solution A dropwise at room temperature under stirring and then the mixture was left for an additional 5 h. The resultant precipitant was washed thoroughly with DI water and isopropanol, and vacuum dried overnight at 60 °C. This resulted in the product denoted as KPB. The Na-containing PBA sample (denoted as NaPB) was synthesized in exactly the same way, except for $K_4Fe(CN)_6 \cdot 3H_2O$ being substituted by $Na_4Fe(CN)_6 \cdot 10H_2O$ and $K_3C_6H_5O_7$ by $Na_3C_6H_5O_7$.

Materials Characterization: The crystal structure of the synthesized powders was identified by Rietveld refinement of X-Ray diffraction (XRD; Stoe STADI P) patterns collected using Mo Kα radiation ($\lambda = 0.7093 \text{ Å}$). The morphology of the products was observed using scanning electron microscopy, energy-dispersive X-ray spectroscopy (SEM, EDS; JEOL

www.advancedsciencenews.com

www.small-structures.com

JSM-JSM-7600F), and transmission electron microscopy (TEM; JEOL JEM-2100). The chemical compositions of the powders were determined using microwave plasma-atomic emission spectroscopy (MP-AES; Agilent 4210 MP-AES), elemental analysis (EA; Thermo Flash 2000) and thermogravimetric analysis (TGA; Netzsch TG 209 F1 Libra, ramp rate of $10\,^{\circ}$ C min $^{-1}$ in N_2 , flow rate 30 mL min $^{-1}$). Infrared spectra were collected using Fourier transform-infrared spectroscopy (FT-IR; Bruker ALPHA compact FT-IR spectrometer). Raman spectra of the powders and electrodes were recorded using a 785 nm laser (Renishaw inVia Raman spectrometer).

Electrochemical Measurement: The working electrodes were composed of 70% PBA sample, 15% KetjenBlack and 15% poly(vinylidene fluoride) (PVDF). The mixture was made into a slurry through the addition of 1-methyl-2-pyrrolidone (NMP). This slurry was coated onto a hydrophobic carbon paper using a drop casting method, before being vacuum dried at 120 °C overnight. The mass loading of the active materials was between 1 and 1.5 mg cm⁻². R2032 type coin cells and three electrode Swagelok cells (SS316 stainless steel pins) were assembled in a glovebox (Ar gas, $O_2 < 0.5$ ppm, $H_2O < 0.5$ ppm). Activated carbon cloth (ACC, Flexzorb FM50K knitted carbon cloth) was used as the counter/reference electrode in coin cells and both counter and reference electrodes in Swagelok cells. Glass fiber membranes (Whatman, GF-B) were used as the separator. A solution of calcium perchlorate $(Ca(ClO_4)_2, 0.5 \text{ M})$ in acetonitrile (ACN) solvent was used as the electrolyte for Ca cells. In the case of K cells, a K metal disk was used as the counter/reference electrode in coin cells, with a solution of potassium perchlorate (KClO₄, 1 M) in ethylene carbonate: propylene carbonate (EC:PC = 1:1 in volume) being used as the electrolyte. In the case of Na cells, a Na metal disk was used as the counter/reference electrode, with a solution of sodium perchlorate (NaClO₄, 1 M) in ethylene carbonate: propylene carbonate (EC:PC = 1:1 in volume) being used as the electrolyte. Galvanostatic charge/discharge (GCD) was performed on a Neware Battery cycler (BTS4000) with a potential window of -0.6-1.1 V versus ACC at various current densities. Cyclic voltammetry (CV) was carried out on a Biologic potentiostat (VSP) with a potential window of -0.6-1.1 V versus ACC at various scan rates. All electrochemical measurements were performed at room temperature. Characterizations of cycled electrodes involved the disassembly of cycled coin cells inside a glovebox where the electrodes were rinsed with ACN. They were then transferred in airtight vessels to avoid atmospheric exposure before characterization.

Computational Method: DFT calculations were performed using the CRYSTAL17 package. [47] A supercell with four $[M_xFeFe(CN)_6]$ (M = Na,K, or Ca) formula units was employed, which has a maximum of eight intercalation sites, under periodic boundary conditions. Calculations were performed in the P_1 space group without any symmetry constraint. Electronic exchange and correlation were described by the PBEO hybrid exchange functional. The use of Hartree-Fock (HF) exchange is necessary to describe the localized nature of *d* electrons on Fe. Commensurate grids for reciprocal space integration were generated, with shrinking factor IS = 4. The default values were used for the truncation of bielectronic integrals (corresponding to TOLINTEG = 7 7 7 7 14), SCF convergence and geometry optimizations. All-electron basis sets of triple zeta plus polarization quality were used for all atoms, retrieved from the CRYSTAL online database using the following tags: (C_m-6-311G(d)_Heyd_2005), $^{[48]}$ (N_m-6-311G(d)_Heyd_2005), $^{[48]}$ (Na_8-511G_dovesi_1991), $^{[49]}$ (K_86-511G_dovesi_1991),^[49] (Ca_86-511d21G_valenzano_2006),^[50] (Fe_86-411d41G_towler_1992a). [51]

The competitive intercalation of monovalent ions ($M^{I} = K$ or Na) or divalent Ca-ion during discharge in CIBs where both M^{+} and Ca^{2+} are dissolved in the electrolyte solution corresponds to the following reaction:

$$M_x^I C a_y P B + A + \Delta \cdot M_{el}^{n+} = M_\Delta M_x^I C a_y P B + A^{\Delta n+}$$
 (1)

where A represents the anode (ACC in this work). $M_x^1Ca_yPB$ and $M_\Delta M_x^1Ca_yPB$ represent the cathode before and after intercalation, respectively. The intercalant M can be K, Na, or Ca. In this reaction, we indicate that the PBA cathode $M_x^1Ca_yPB$ may contain some pre-intercalated amount of M^+ or Ca^{2+} . The competitive intercalation of an amount, Δ , of M^{n+}

(Na, K, Ca) into the cathode is considered, with these ions sourced from the electrolyte ($M_{\rm el}^{n+}$) and balanced by the desorption of ions with overall $\Delta \cdot n+$ charge from the anode.

We investigate how the intercalation energy per unit of charge, $E_{\rm M}^i$, depends on the initial composition of the cathode, $M_{\rm x}^I {\rm Ca}_{\rm y} {\rm PB}$, through the equation:

$$E_{\mathbf{M}}^{i}(\mathsf{M}_{x}^{i}\mathsf{Ca}_{y}\mathsf{PB}) = \frac{1}{\Delta \cdot n} [E(\mathsf{M}_{\Delta}\mathsf{M}_{x}^{i}\mathsf{Ca}_{y}\mathsf{PB}) + E(\mathsf{A}^{\Delta n+}) \\ - E(\mathsf{M}_{x}^{i}\mathsf{Ca}_{y}\mathsf{PB}) - E(\mathsf{A}) - \Delta \cdot E(\mathsf{M}_{a}^{n+})]$$
(2)

The energies of solvated Na, K, and Ca, $E(M_{el}^{n+})$, were derived from a thermodynamic cycle using the following equation:

$$E(M_{el}^{n+}) = E(M_{g}^{n+}) - E_{\text{ionization}}(M) - E_{\text{cohesive}}(M) + neV_{cell}^{\Theta}(M)$$
(3)

where $E(M_n^{m^+})$ is the energy of an isolated M^{n^+} calculated using the same functional, basis set and numerical parameters as the PB materials, $V_{\text{cell}}^{\Theta}(M)$ is the standard reduction potential of metal M corresponding to the reaction $M_{\text{aq}}^{n^+} + \text{ne}^- \to M$. $E_{\text{ionization}}(M)$ and $E_{\text{cohesive}}(M)$ are the ionization potential and cohesive energy, linking the energy M^{n^+} to that of solid M. [52–54]

The barriers of ion migration in PBA structure were calculated using constrained geometry optimizations. A series of configurations were used with the chosen migrating ion located at different x coordinates through the sub-cubes in the supercell and along the <100> migration direction. Energy barrier and migration pathway are utilized to compare the mobility of different ions in the PB cathode structure.

Supporting Information

Supporting Information is available from the Wiley Online Library or from the author.

Acknowledgements

Y.X. acknowledges the financial support of the Engineering and Physical Sciences Research Council (EP/X000087/1, EP/V000152/1), Leverhulme Trust (RPG-2021-138), Royal Society (IEC\NSFC\223016), and Science and Technology Facilities Council Batteries Network (ST/R006873/1). The authors acknowledge the use of the UCL Kathleen High Performance Computing Facility (Kathleen@UCL), and associated support services, in the completion of this work. For the purpose of open access, the authors have applied for a Creative Commons Attribution (CC BY) license to any author-accepted manuscript version arising.

Conflict of Interest

The authors declare no conflict of interest.

Author Contributions

Henry R. Tinker: Conceptualization (equal); Data curation (lead); Methodology (lead); Writing—original draft (lead). Mingrui Li: Data curation (supporting); Formal analysis (supporting); Writing—review & editing (supporting). Ajay Piriya Vijaya Kumar Saroja: Data curation (supporting); Formal analysis (supporting); Methodology (supporting); Validation (supporting). Yuhan Liu: Formal analysis (supporting); Validation (supporting). Yudong Luo: Data curation (supporting). Wanjun Ren: Data curation (supporting); Formal analysis (supporting); Methodology (supporting). Runzhe Wei: Formal analysis (supporting); Methodology (supporting). Yi Lu: Formal analysis (supporting). Pan He: Formal analysis (supporting). Yupei Han: Formal analysis (supporting).

www advancedsciencenews com

www.small-structures.com

Christopher A. Howard: Data curation (supporting); Methodology (supporting); Resources (supporting). Furio Corà: Conceptualization (equal); Data curation (supporting); Formal analysis (supporting); Supervision (supporting); Writing—review & editing (equal). Yang Xu: Conceptualization (lead); Formal analysis (supporting); Funding acquisition (lead); Project administration (lead); Supervision (lead); Validation (lead); Writing—original draft (equal); Writing—review & editing (lead).

Data Availability Statement

The data that support the findings of this study are available from the corresponding author upon reasonable request.

Keywords

Ca-ion battery, electrochemical mechanism, hybrid battery, intercalation, Prussian blue analogues, sustainable energy storage

Received: June 20, 2024 Revised: September 4, 2024 Published online: September 30, 2024

- N. Yabuuchi, K. Kubota, M. Dahbi, S. Komaba, Chem. Rev. 2014, 114, 11636
- [2] T. Hosaka, K. Kubota, A. S. Hameed, S. Komaba, Chem. Rev. 2020, 120. 6358.
- [3] Y. Xu, M. Titirici, J. Chen, F. Cora, P. L. Cullen, J. S. Edge, K. Fan, L. Fan, J. Feng, T. Hosaka, J. Phys.: Energy 2023, 5, 021502.
- [4] Y. Liang, H. Dong, D. Aurbach, Y. Yao, Nat. Energy 2020, 5, 646.
- [5] M. E. Arroyo-de Dompablo, A. Ponrouch, P. Johansson, M. R. Palacín, Chem. Rev. 2019, 120, 6331.
- [6] M. Li, J. Lu, X. Ji, Y. Li, Y. Shao, Z. Chen, C. Zhong, K. Amine, Nat. Rev. Mater. 2020, 5, 276.
- [7] M. Mao, T. Gao, S. Hou, C. Wang, Chem. Soc. Rev. 2018, 47, 8804.
- [8] H. R. Tinker, C. A. Howard, M. Zhou, Y. Xu, Mater. Adv. 2023, 4, 2028.
- [9] J. Tu, W.-L. Song, H. Lei, Z. Yu, L.-L. Chen, M. Wang, S. Jiao, Chem. Rev. 2021, 121, 4903.
- [10] Y. Wu, Z. Zhao, X. Hao, R. Xu, L. Li, D. Lv, X. Huang, Q. Zhao, Y. Xu, Y. Wu, Carbon Neutralization 2023, 2, 551.
- [11] E. Faegh, B. Ng, D. Hayman, W. E. Mustain, Nat. Energy 2021, 6, 21.
- [12] A. A. Yaroshevsky, Geochem. Int. 2006, 44, 48.
- [13] A. Ponrouch, C. Frontera, F. Bardé, M. R. Palacín, Nat. Mater. 2016, 15, 169.
- [14] A. Ponrouch, J. Bitenc, R. Dominko, N. Lindahl, P. Johansson, M. R. Palacín, Energy Storage Mater. 2019, 20, 253.
- [15] B. Jeon, H. H. Kwak, S.-T. Hong, Chem. Mater. 2022, 34, 1491.
- [16] Z.-L. Xu, J. Park, J. Wang, H. Moon, G. Yoon, J. Lim, Y.-J. Ko, S.-P. Cho, S.-Y. Lee, K. Kang, *Nat. Commun.* **2021**, *12*, 3369.
- [17] T. Shiga, H. Kondo, Y. Kato, M. Inoue, J. Phys. Chem. C 2015, 119, 27946.
- [18] C.-Y. Du, Z.-H. Zhang, X.-L. Li, R.-J. Luo, C. Ma, J. Bao, J. Zeng, X. Xu, F. Wang, Y.-N. Zhou, Chem. Eng. J. 2023, 451, 138650.
- [19] Z. Meng, A. Reupert, Y. Tang, Z. Li, G. Karkera, L. Wang, A. Roy, T. Diemant, M. Fichtner, Z. Zhao-Karger, ACS Appl. Mater. Interfaces 2022, 14, 54616.
- [20] D. S. Tchitchekova, A. Ponrouch, R. Verrelli, T. Broux, C. Frontera, A. Sorrentino, F. Bardé, N. Biskup, M. E. Arroyo-de Dompablo, M. R. Palacin, *Chem. Mater.* 2018, 30, 847.
- [21] T. N. Vo, J. Hur, I. T. Kim, ACS Sustainable Chem. Eng. 2020, 8, 2596.
- [22] D. Bier, Z. Li, S. Klyatskaya, N. Sbei, A. Roy, S. Riedel, M. Fichtner, M. Ruben, Z. Zhao-Karger, ChemSusChem 2023, 16, e202300932.

- [23] N. M. Vargas-Barbosa, Nat. Nanotechnol. 2024, 19, 419.
- [24] C. Zhang, Y. Xu, M. Zhou, L. Liang, H. Dong, M. Wu, Y. Yang, Y. Lei, Adv. Funct. Mater. 2017, 27, 1604307.
- [25] R. Wei, X. Zhai, H. R. Tinker, P. He, C. A. Nason, Y. Han, V. Celorrio, G. Sankar, M. Zhou, Y. Xu, Adv. Funct. Mater. 2023, 33, 2308227.
- [26] M. S. Chae, J. Hyoung, M. Jang, H. Lee, S.-T. Hong, J. Power Sources 2017, 363, 269.
- [27] L. Reed, S. Ortiz, M. Xiong, E. Menke, Chem. Commun. 2015, 51, 14397.
- [28] N. Kuperman, P. Padigi, G. Goncher, D. Evans, J. Thiebes, R. Solanki, J. Power Sources 2017, 342, 414.
- [29] T. N. Vo, J. E. Kang, H. Lee, S. W. Lee, S. K. Ahn, J. Hur, I. T. Kim, EcoMat 2023, 5, e12285.
- [30] R. Y. Wang, C. D. Wessells, R. A. Huggins, Y. Cui, Nano Lett. 2013, 13, 5748.
- [31] T. Tojo, Y. Sugiura, R. Inada, Y. Sakurai, Electrochim. Acta 2016, 207, 22
- [32] C. Lee, S.-K. Jeong, Electrochemistry 2018, 86, 134.
- [33] A. L. Lipson, B. Pan, S. H. Lapidus, C. Liao, J. T. Vaughey, B. J. Ingram, Chem. Mater. 2015, 27, 8442.
- [34] A. L. Lipson, S.-D. Han, S. Kim, B. Pan, N. Sa, C. Liao, T. T. Fister, A. K. Burrell, J. T. Vaughey, B. J. Ingram, J. Power Sources 2016, 325, 646.
- [35] T. Hosaka, T. Fukabori, H. Kojima, K. Kubota, S. Komaba, ChemSusChem 2021, 14, 1166.
- [36] X. Bie, K. Kubota, T. Hosaka, K. Chihara, S. Komaba, J. Mater. Chem. A 2017. 5, 4325.
- [37] Y. Liu, S. Fan, Y. Gao, Y. Liu, H. Zhang, J. Chen, X. Chen, J. Huang, X. Liu, L. Li, Y. Qiao, S. Chou, Small 2023, 19, 2302687.
- [38] S. N. Ghosh, J. Inorg. Nucl. Chem. 1974, 36, 2465.
- [39] S. Wheeler, I. Capone, S. Day, C. Tang, M. Pasta, Chem. Mater. 2019, 31, 2619.
- [40] D. B. Brown, D. F. Shriver, Inorg. Chem. 1969, 8, 37.
- [41] R. Mažeikienė, G. Niaura, A. Malinauskas, J. Electroanal. Chem. 2014, 719. 60.
- [42] G. Moretti, C. Gervais, J. Raman Spectrosc. 2018, 49, 1198.
- [43] Y. Qi, V. Brasiliense, T. W. Ueltschi, J. E. Park, M. R. Wasielewski, G. C. Schatz, R. P. Van Duyne, J. Am. Chem. Soc. 2020, 142, 13120.
- [44] W.-J. Li, S.-L. Chou, J.-Z. Wang, Y.-M. Kang, J.-L. Wang, Y. Liu, Q.-F. Gu, H.-K. Liu, S.-X. Dou, Chem. Mater. 2015, 27, 1997.
- [45] A. Zhou, W. Cheng, W. Wang, Q. Zhao, J. Xie, W. Zhang, H. Gao, L. Xue, J. Li, Adv. Energy Mater. 2021, 11, 2000943.
- [46] B. Yan, M. Li, X. Li, Z. Bai, J. Yang, D. Xiong, D. Li, J. Mater. Chem. A 2015, 3, 11773.
- [47] R. Dovesi, A. Erba, R. Orlando, C. M. Zicovich-Wilson, B. Civalleri, L. Maschio, M. Rérat, S. Casassa, J. Baima, S. Salustro, B. Kirtman, WIREs Comput. Mol. Sci. 2018, 8, e1360.
- [48] J. Heyd, J. E. Peralta, G. E. Scuseria, R. L. Martin, J. Chem. Phys. 2005, 123, 174101.
- [49] R. Dovesi, C. Roetti, C. Freyria-Fava, M. Prencipe, V. Saunders, Chem. Phys. 1991, 156, 11.
- [50] L. Valenzano, F. J. Torres, K. Doll, F. Pascale, C. M. Zicovich-Wilson, R. Dovesi, Z. Phys. Chem. 2006, 220, 893.
- [51] M. Catti, G. Valerio, R. Dovesi, Phys. Rev. B 1995, 51, 7441.
- [52] C. Kittel, Introduction to Solid State Physics, 8th ed., John Wiley & Sons, Inc., Hoboken, NJ 2005.
- [53] W. M. Haynes, CRC Handbook of Chemistry and Physics, 97th ed., CRC Press, Boca Raton 2016.
- [54] A. M. W. C. Martin, S. Kotochigova, J. E. Sansonetti, Ground Levels and Ionization Energies for the Neutral Atoms, National Institute of Standards and Technology, Gaithersburg, MD 2013.